Applied Surface Science 255 (2009) 6598–6606

Contents lists available at ScienceDirect

Applied Surface Science

journal homepage: www.elsevier.com/locate/apsusc

Bulk and surface plasmon excitations in amorphous carbon measured by core-level photoelectron spectroscopy

Christian Godet [a,*], Denis David [b], Hussein Sabbah [a], Soraya Ababou-Girard [a], Francine Solal [a]

[a] Physique des Surfaces et Interfaces, Institut de Physique de Rennes (CNRS UMR 6251), Université Rennes 1, Beaulieu 35042 Rennes, France
[b] Instituto de Fisica, Universidade Federal da Bahia, Campus Universitário de Ondina, 40.210-340 Salvador, Bahia, Brazil

ARTICLE INFO

Article history:
Received 8 December 2008
Received in revised form 30 January 2009
Accepted 15 February 2009
Available online 23 February 2009

PACS:
73.20.Mf
73.60.Ht
68.35.bj
82.80.Pv

Keywords:
Plasmon
XPS
Amorphous carbon
Organic molecular layer

ABSTRACT

Bulk and surface plasmon excitations in amorphous carbon (a-C) films have been characterized by core-level loss spectroscopy. Atomically smooth a-C surfaces were used in their as-grown state, after UHV annealing and after covalent immobilization of dense molecular monolayers ($2–4 \times 10^{14}$ cm^{-2}), either perfluorinated or labelled with an ester functionality. X-ray photoelectron spectra reveal a sp^3-rich hybridization of surface C atoms, with a $\sigma + \pi$ plasmon loss distribution centred at 29.5 ± 1 eV, characteristic of a high electron density value. For molecular grafted surfaces, the energy distribution of plasmon losses reveals new contributions in the range 15–25 eV (clearly separated from the energy distribution of the bulk $\sigma + \pi$ plasmon loss of a-C) with an increasing loss probability observed at grazing photoemission angles. A simple parameterization method is presented to derive bulk and surface plasmon loss distributions from angular core level loss spectroscopy (XPS) data, without *a priori* assumptions on the shape of the loss energy distributions.

1. Introduction

Amorphous carbon (a-C) and its alloys are interesting thin film materials due to their outstanding properties, such as high hardness, good tribological properties, chemical inertness and biocompatibility [1–6]. In addition to their applications as protective coatings and solid lubricants, a-C films have emerged as electrodes for analytical electrochemistry due to their large overpotential in aqueous solvent [7] and as injecting electrodes for organic light emitting diodes [8]. Efficient covalent grafting of molecular species to a-C surfaces has been developed to design selective sensors for biomolecular recognition [9,10].

In spite of this technological importance of amorphous carbon surfaces, a clear and comprehensive picture of the relationship between their chemical, physical and electronic properties is still lacking. To this end, non-destructive surface characterizations such as X-ray Photoelectron Spectroscopy (XPS), combined with electron energy loss spectroscopy, are thus highly valuable provided that clear signatures of bulk and surface responses can be identified.

In contrast, the physical and structural properties of bulk a-C films have been extensively studied in relation with thin film deposition and processing conditions. In particular, the density and average hybridization of C atoms, which control hardness and electronic structure properties, can be tailored by adjusting the energy of C^+ ions in the so-called subplantation growth mode [1,11,12]. Electron energy loss spectroscopy (EELS) is currently considered as the most reliable technique to determine the density of a-C films. In the field of carbon-based materials, the $\sigma + \pi$ plasmon has been widely used as a useful signature for process control [4,13–21], for a simple calibration of the sp^3 content [15,16,22,23], and for the analysis of complex phase mixtures or interfaces [24–28].

Because of the collective nature of plasmon losses, the low-loss spectrum is best described in terms of the complex dielectric function, $\varepsilon(E)$, of the medium [29–37]. Hence EELS is a powerful tool to obtain the dielectric function over a wide energy range, either in transmission (TEELS [29,38]) or in reflection (REELS [39–42]) geometries. For the same a-C sample, the bulk sensitive TEELS (fast electrons, $E_0 > 10$ keV) and surface sensitive REELS (low energy electrons, $E_0 < 1$ keV) may provide different atom density values because bulk and surface properties of sp^3-rich a-C films can

* Corresponding author at: EPSI–IPR, Université Rennes 1, Bât. 11C - Beaulieu, 35042 Rennes, France. Tel.: +33 2 23 23 57 06; fax: +33 2 23 23 61 98.
E-mail address: christian.godet@univ-rennes1.fr (C. Godet).

0169-4332/$ – see front matter © 2009 Elsevier B.V. All rights reserved.
doi:10.1016/j.apsusc.2009.02.050

be quite different, e.g. a larger surface sp^2 fraction has been evidenced in spatially resolved EELS [43] and confirmed by Monte Carlo simulations [12].

The physics and surface sensitivity of plasmon losses in XPS and REELS are similar in principle, except for the presence of the electron–hole interaction and the lack of collimated beam in XPS. However, very few XPS studies have focused on core-level loss spectroscopy in amorphous carbon films [44–46]. In addition, for amorphous semiconductors, surface plasmon losses are usually too weak to be observed in XPS [44,45,47] or EELS [48] measurements.

In this work, bulk and surface plasmon excitations of amorphous carbon thin films have been observed and investigated as a function of the photoelectron emission angle, using a conventional XPS instrument. Section 2 recalls the physics of bulk and surface plasmon losses and describes the derivation of normalized core level loss distributions from XPS data. Section 3 gives experimental details on the a-C film deposition and surface modifications. Pulsed Lased Deposited (PLD) a-C films, chosen for their high $sp^3/(sp^2 + sp^3)$ hybridization [46] and their very smooth surfaces [49] were characterized either in their as-grown state, or after UHV annealing. In order to obtain a surface chemical label for the separation of bulk vs surface plasmon losses, a densely packed monolayer of organic linear chains has been covalently immobilized on as-deposited a-C surfaces, using thermally assisted grafting of linear alkene molecules, either perfluorinated (CF_2 and CF_3 in C1s spectra) or bearing ester functionalities (O=C–O in C1s spectra).

In Section 4, core-level loss spectroscopy is used to characterize the near-surface electron density derived from the $\sigma + \pi$ plasmon losses, and the structural organization of the sp^2 phase derived from the π plasmon feature, observed in as-deposited and annealed a-C films. Difference spectra are considered to evaluate the effects of the baseline subtraction procedure and possible shifts in the binding energy, e.g. due to band bending. For molecular grafted a-C surfaces, core-level loss spectroscopy shows an increasing total loss probability as the photoelectron emission approaches grazing incidence. The angular dependence of inelastic losses is analyzed in order to separate the contributions of bulk vs surface plasmon losses; the proposed parameterization is validated using monolayer grafting of chemically labelled alkene molecules. Finally, the origin of the strong surface loss probability found in a-C with a dense covalently immobilized molecular layer (as compared to the pristine and annealed a-C) is discussed in Section 5.

2. Core level loss data analysis

2.1. Surface and bulk plasmon excitations

Electrons which pass through a solid interact with the free and bound electrons. Collective excitations run as longitudinal charge density fluctuations through the volume of the solid (volume plasmon) and along its surface (surface plasmon). Their energy, $E = \hbar\omega$, is related to the frequency ω of oscillation; it depends on the density of loosely bound electrons, i.e. those for which $\hbar\omega_P$ (ω_P plasma frequency) is large compared with their binding energy (in semiconductors the electrons in the valence band).

In XPS experiments, due to the small absorption coefficient of X-ray excitation, electron–hole pairs are created homogeneously in the film, over several microns. An electron–hole pair creates an induced charge-density in the medium during photoexcitation (intrinsic loss) and electron transport (extrinsic loss). The origin of the electron energy loss is that the induced electric field in the medium acts on the electron as it moves [29–37].

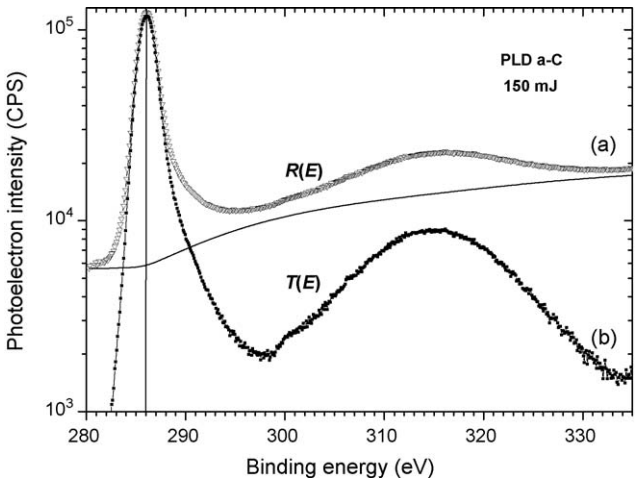

Fig. 1. C1s core level spectrum (log scale) at normal emission angle ($\alpha = 0°$) for a PLD a-C film (150 mJ): (a) raw measurements, $R(E)$; (b) $T(E)$, after subtraction of a Tougaard universal background function [51,52] (continuous line).

In amorphous carbon, the C1s line at a binding energy $E_B \approx 285$ eV is followed by a structured background of electrons extending towards higher binding (lower kinetic) energies (Fig. 1). This broad loss spectrum corresponds to C1s photoelectrons that have suffered energy losses on the way from their point of creation to the sample surface (and across the sample surface) and it is thus characteristic for the sample under investigation. For high-energy primary photoelectrons ($E_0 > 300$ eV), losses in the energy range $\hbar\omega = 5–50$ eV are dominated by the creation of bulk plasmons, and the energy $\hbar\omega_{max}$ of the maximum in the loss spectrum is commonly identified with the plasmon energy $\hbar\omega_P$ (Fig. 2). The loss spectrum of a-C displays loss features at 5–6 eV and 23–30 eV, respectively attributed to the π and $\sigma + \pi$ plasmon losses [22,23,38,40–42,46].

The usual quantity to describe the energy loss is the product of the inelastic cross-section by the atom density, $K(E_0, \hbar\omega)$, which gives the probability density per unit path length of losing an energy $\hbar\omega$. Because of the collective nature of plasmon losses, the low-loss spectrum is best described in terms of the complex dielectric function, $\varepsilon(\hbar\omega)$, of the solid. For electrons travelling through an *infinite* medium, it is given by [30–36]:

$$K(E_0, \hbar\omega) = (E_0 \pi a_0)^{-1} \int \mathrm{d}k\, k^{-1} \mathrm{Im}\left(\frac{-1}{\varepsilon(\hbar\omega)}\right), \quad (1)$$

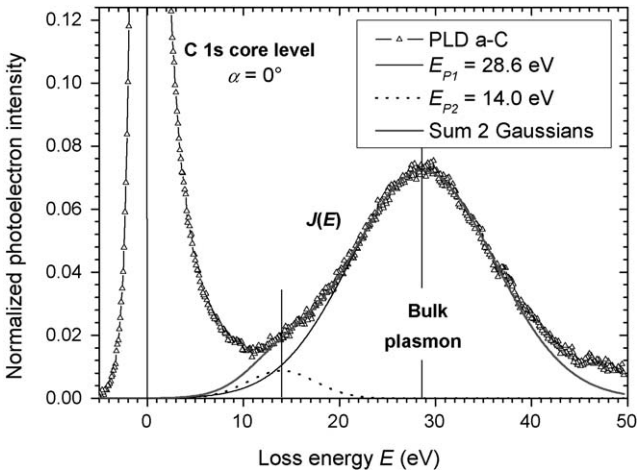

Fig. 2. Normalized loss, $J(E)$, at normal emission angle ($\alpha = 0°$) for a PLD a-C film (180 mJ) and fitting (in the range 13.7–34.7 eV) with a sum of two Gaussians centered at 14.0 and 28.6 eV.

where E_0 is the initial kinetic energy of the electron, a_0 is the Bohr radius, and k is the wave vector transferred from the electron. $k\pm = (2m/\hbar^2)^{1/2}[E_0^{1/2} \pm (E_0 - \hbar\omega)^{1/2}]$ are the limits on the k vector imposed by energy and momentum conservation during the inelastic scattering. The inelastic mean free path for plasmon losses, λ_P, is defined by:

$$\lambda_P(E_0)^{-1} = \int \mathrm{d}\hbar\omega\, K(E_0, \hbar\omega) \quad (2)$$

However, an additional unstructured inelastic background at low energies (0–10 eV) results from single particle losses, such as electron–electron interactions [50–54], so that a total inelastic cross section should be considered:

$$\lambda(E_0)^{-1} = \lambda_P(E_0)^{-1} + \lambda_E(E_0)^{-1} \quad (3)$$

The bulk plasmon intensity (A_{BP}) normalized to the elastic peak intensity (A_{EL}) is given by $(A_{BP}/A_{EL}) = \lambda/\lambda_P$ [55].

Collective excitations of electrons exist not only in the volume of a plasma but also in its boundary. Longitudinal waves of the surface charge density are possible which run along the surface as a polarisation wave. However, Eq. (1) does not reproduce the surface loss features observed in REELS and XPS which correspond to an additional term proportional to $Im\,[-1/(1+\varepsilon(E))]$ [29,31,35,36]. Alternatively, the surface loss distribution is integrated to derive the so-called surface excitation parameter (SEP) which is the average number of surface excitations an electron experiences when it crosses the surface once [56,57]. Recent works have addressed the difficult problem of the separation of surface and bulk plasmons, which contribute to experimental losses, either from a linear combination of $[-1/\varepsilon(E)]$ and $[-1/(1+\varepsilon(E))]$, or from direct calculations using the dielectric function of the medium as the input parameter [39,40,58–67].

As shown in previous XPS studies of metal and Si surfaces, the increase of losses for glancing emission is essentially sensitive to the surface plasmon properties rather than to bulk losses [63,68]. This work addresses experimentally the problem of surface vs bulk plasmon excitations using the angular dependence of the energy distribution of photoelectron losses in XPS spectra.

2.2. Data analysis

In this study, the normalized photoelectron loss intensity $J(E)$ provides evidence of surface losses in addition to the usual bulk plasmon losses. Core level loss spectra, measured at different emission angles (α = 0–75°), are used for the separation of bulk vs surface contributions, using the pure surface contribution provided by a chemical functionality (ester, CF_2, CF_3) within the molecular monolayer.

We have used the following procedure for XPS data treatment: (a) a Tougaard "universal" background for bulk inelastic scattering events [51–54] is subtracted from raw XPS data, $R(E)$ (see Section 3.5) providing the corrected spectrum $T(E)$ (Fig. 1); (b) $T(E)$ is normalized to the elastic peak maximum, providing $J(E)$ (Fig. 2); (c) since a single asymmetric lineshape cannot describe properly all our measurements, a decomposition of the normalized photoelectron loss intensity, $J(E)$, into Gaussians is performed by tentatively setting a constant position for all emission angles α; (d) the angular dependence of their integrated intensities is used to attribute a physical origin to each component and to separate "pure bulk" and "pure surface" losses.

The angular dependence of the high loss energy (25–35 eV) component being negligible, it will be attributed to a bulk component. In contrast, the angular dependence of the component at low loss energy (15–25 eV) being proportional to $1/\cos\alpha$, similar to the behaviour of molecular functionalities, it will be attributed to a surface component. This behaviour being observed on several amorphous carbon films, covalently grafted using either a liquid phase or a gas phase process, we will tentatively parameterize the angular dependence of the lineshape of the normalized loss by $J(E) = B(E) + S(E)(\cos\alpha)^{-1}$. The consistency of this approximation will be checked by extracting the "pure bulk" $B(E)$ and "pure surface" $S(E)$ losses for different couples of angles, typically (0, 45°) and (0, 55°). Note that $J(E)$ and $B(E)$ both include the elastic peak distribution $Z(E)$.

3. Experimental methods

3.1. Deposition process

Carbon films (30–60 nm-thick) have been grown at room-temperature by pulsed laser deposition (PLD) using a KrF laser (Tuilaser Excistar λ = 248 nm, 2 Hz, 20 ns pulse width) in a turbo-pumped high vacuum chamber (base pressure ~10^{-4} Pa).

After ultrasonic bath cleaning in acetone, isopropanol and water (111) crystalline silicon (c-Si) substrates were placed at 40 or 60 mm from a rotating glassy carbon target (Sigradur G, HTW). The impact area on the target being 2.20 mm × 0.75 mm, the maximum pulse energy (200 mJ) corresponds to a fluence of ~10 J cm^{-2}. Before deposition, the target was cleaned for 5 min at 2 Hz with a shutter in front of the substrate. After deposition, nitrogen was introduced in the chamber and the carbon film was quickly transferred to the XPS setup or to the grafting setup under a dry nitrogen atmosphere.

Under these optimized conditions, we checked that no micron-sized pieces ejected from the target were present on the a-C film surface [49]. Scanning Electron Microscopy images of optimized films still show some droplets (typical size 30–50 nm diameter) on the a-C surface, which cover less than 0.2% of the film surface. In addition, AFM analysis provides an average roughness of 0.2–0.3 nm on 2 μm × 2 μm images. This PLD a-C surface is thus suitable for molecular grafting and surface plasmon studies.

3.2. Annealing

The thermal stability of PLD a-C surfaces being important for thermally assisted grafting processes, a carbon film (35 nm-thick) grown on a (111) silicon surface has been annealed under UHV (10^{-5} Pa) on a resistively heated thermally conducting holder. Successive annealing steps at increasing temperatures (270, 330, 420, 520, 610 °C) have been performed. The lower temperatures were calibrated using the melting point of In (T_{melt} = 157 °C) and Sn (T_{melt} = 232 °C), while a pyrometer has been used above 300 °C. The temperature rising time is about 0.5 h and the annealing time is 0.5 h.

3.3. Liquid phase thermal grafting method

A low-temperature (160 °C) liquid-phase thermal process described previously [10] was used to react linear ethyl undecylenate $CH_2{=}CH(CH_2)_8{-}COOC_2H_5$ molecules with a-C surfaces. Briefly, ethyl undecylenate (Aldrich, 97%) was passed through a neutral, activated alumina column to remove residual water and peroxides, and was further deoxygenated at 160 °C for at least 2 h before substrate introduction. After overnight exposure at 160 °C, and cooling, the modified surfaces were rinsed copiously to eliminate physisorbed molecules before XPS characterization.

3.4. Gas phase thermal grafting method

A gas-phase thermally induced process was used to immobilize linear perfluorodecene $CH_2{=}CH(CF_2)_7CF_3$ molecules on as-deposited a-C film surfaces. The grafting setup has been described

elsewhere [49,69]. The perfluorodecene vapour was introduced into the UHV chamber containing the heated a-C film, evacuated with a diffusion pump (1×10^{-6} Pa). After closing the evacuation valve, the PFD pressure (~20 Pa) was maintained for 1 h or 2 h for grafting at temperature $T_G = 230$ °C. In order to remove physisorbed molecules, grafted surfaces were further annealed (30 min in UHV) at $T_A = 230$ °C. It has been checked that this thermal process in UHV is efficient to remove most physisorbed PFD molecules [69].Sangeeta

3.5. Sangeeta In situ XPS and plasmon analysis

After a few minutes at the ambient, as-deposited or grafted surfaces were introduced in the UHV chamber and kept at 10^{-6} Pa for a few hours before XPS analysis. Measurements were performed with a Mg Kα ($h_\nu = 1253.6$ eV) X-ray source, using a VSW HA100 photoelectron spectrometer (electron analyzer HAC 100). By rotating the sample, angular analysis could be performed from $\alpha = 0°$ (normal) to 75° emission angles, with a constant detection angle of 54.7°.

Molecular coverage values of the grafted surfaces were deduced from O=C–O, CF_2 and CF_3 intensities in C1s spectra (normalized to the C1s intensity of a clean HOPG surface) taken with a 1.0 eV resolution and a typical count rate of 8×10^5 counts eV^{-1}, at the C1s core level peak. Spectral analysis included a Shirley background subtraction [50] and peak separation using mixed Gaussian–Lorentzian functions. For hybridization analysis, monochromatic Al Kα ($h\nu = 1486.6$ eV) excitation was used, with an energy resolution of 0.6 eV at constant pass-energy (10 eV) and a typical count rate of 8×10^4 counts eV^{-1}, for the C1s core level (full width at half maximum FWHM = 1.7 eV).

For core-level loss spectroscopy, plasmon losses were measured with a 1.3 eV resolution, with a typical count rate of 8×10^4 counts eV^{-1}, near the plasmon loss peak maximum at $E_P = \hbar\omega_P$. The zero-loss peak is thus slightly broadened, with an apparent full width FWHM ≅ 2.1 eV. A Tougaard inelastic background [51,52], using the universal cross section $\lambda_P\ (E_0)\ K(E_0, \hbar\omega) = B\ \hbar\omega\ (C + (\hbar\omega)^2)^{-2}$ with $C = 1643$ eV^2 and $B \cong 2866$ eV^2, was subtracted from raw data (Fig. 1) over a 50 eV range to eliminate the unstructured loss background. The loss spectrum $J(E)$ is obtained after normalization of $T(E)$ to the maximum of the elastic peak (Fig. 2). Owing to the possible occurrence of two-fold and higher order multiple plasmon losses (at high E) and surface plasmon losses (at low E), the plasmon lineshape in the range 5–50 eV has been analyzed using a sum of Gaussian components to account for the surface and bulk contributions.

4. Results and discussion

4.1. As-deposited a-C surfaces

Surface roughness is an important parameter for surface plasmon investigations. A typical a-C film (150 mJ laser intensity, 60 mm target distance, $sp^3/(sp^2 + sp^3) = 0.62 \pm 0.01$) grown on crystalline silicon has been characterized using Atomic Force Microscopy (AFM), spectroscopic ellipsometry (SE) and X-ray reflectometry (XRR) [49]. XRR data analysis provide a surface roughness value, $d_R = 0.33$ nm, consistent with AFM measurements (0.2–0.3 nm roughness). The average bulk density of the a-C film is $\rho_{a\text{-}C} = 2.93$ g cm^{-3}. The bulk refractive index, n (2 eV) > 2.6, is characteristic of a high density material, as usually observed for a-C films grown using nanosecond PLD [70].

XPS data show a surface contamination with oxygen atoms (≈5 O at.%) along with some incorporation of nitrogen (<0.6 N at.%) in the as-deposited a-C films. A decomposition of C1s spectra into two Voigt bands provides the average binding energy and width of the corresponding sp^2 and sp^3 hybridizations [46]. A weak third band at higher binding energy is due to oxidized carbon atoms. The difference in binding energies is $E_B(sp^3) - E_B(sp^2) = 0.82 \pm 0.05$ eV. The average surface hybridization values, $sp^3/(sp^2 + sp^3)$ in the range 0.45–0.70, reveal sp^3-rich a-C films.

4.2. Annealing

After each annealing step, the surface was characterized *in situ* by XPS, showing a first departure of oxygen at 320 °C, attributed to carboxylic acid (O=C–OH) functionalities, and elimination of the remaining oxygen at 610 °C, attributed to carbonyl (C=O) moieties [71]. Starting from an initial average hybridization ($sp^3/sp^2 + sp^3$) = 0.48, monochromatic XPS data show a weak decrease of the sp^3 content between 270 and 420 °C, followed by a stronger change above 520 °C; one obtains ($sp^3/sp^2 + sp^3$) = 0.33 after the final annealing step at 610 °C.

The C1s photoelectron spectra at normal emission angle ($\alpha = 0°$) for a PLD a-C film were measured in the as-deposited state and after annealing at 610 °C (Fig. 3). The difference spectrum, J(a-C annealed) − J(a-C), shows an enhanced π plasmon contribution (at 5.5 eV), consistent with the increase in the near-surface sp^2 fraction; it probably reveals a better ordering of the polyaromatic sp^2 phase.

Interestingly, the loss intensity is unchanged between 10 and 50 eV; this lack of any detectable change in the (σ + π) plasmon energy distribution after UHV annealing at 610 °C shows that dense sp^3-rich a-C films are thermally stable [4]. After annealing, a very small decrease of surface plasmon losses is detected in the range 13–20 eV, in contrast with the significant increase reported in the next Section for the molecular grafting of a-C surfaces.

4.3. Molecular grafting

In the following, the angular dependence of the core level loss spectra is analyzed in detail for the ester-functionalized molecular layer. Fig. 4 shows the C1s photoelectron spectra at normal emission angle ($\alpha = 0°$) for the PLD a-C film before and after grafting. The ester O–C=O function appears in the XPS spectra of the grafted a-C surface (at 4.1 eV from the C–C main peak), providing the surface coverage $\Sigma_{ML} = 3.7 \times 10^{14}$ cm^{-2}. The difference spectrum, J(a-C + ester) − J(a-C), shows that the loss intensity near 5.5 eV (π plasmon) is depressed while the region 15–25 eV is enhanced after molecular grafting.

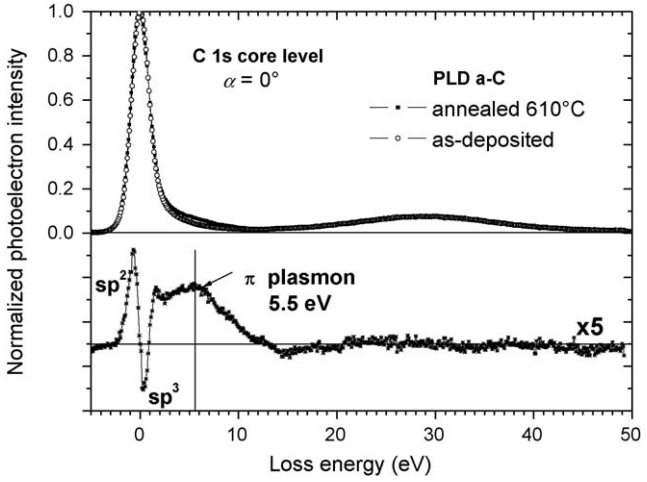

Fig. 3. Top: normalized C1s photoelectron loss spectra ($\alpha = 0°$) for a PLD a-C film (150 mJ) before and after annealing at 610 °C (30 min). Bottom: the difference spectrum, J(a-C annealed) − J(a-C), shows an enhanced π plasmon contribution (at 5.5 eV) while the loss remains unchanged between 12 and 50 eV (including the σ + π plasmon loss range).

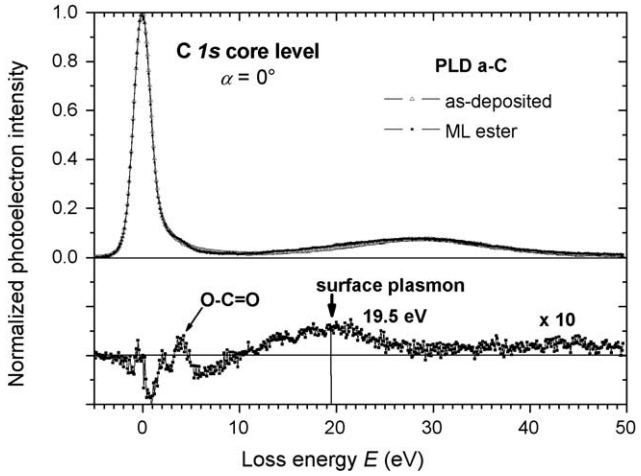

Fig. 4. Top: normalized C1s photoelectron loss spectra ($\alpha = 0^\circ$) for a PLD a-C film before and after grafting an ester-functionalized molecular layer (surface coverage $\Sigma_{ML} = 3.7 \times 10^{14}\,cm^{-2}$). Bottom: the difference spectrum J(a-C + ester) − J(a-C) shows an increase in the surface plasmon component (19.5 eV) along with the ester signature.

A systematic angular analysis has been performed in order to identify the physical origin and to quantify the new loss features. We will show below that the new loss features in the range 15–25 eV can be attributed to surface losses. Fig. 5a shows the bare a-C losses ($\alpha = 0^\circ$) and the angular dependence of losses in the ester grafted a-C surface. The normalized spectra shown in Fig. 5a have been used to obtain the difference spectra $J(\alpha) - J(\alpha = 0^\circ)$ (Fig. 5b). Increasing emission angles enhance the C1s photoelectron bands due to the ester O–C═O function (4.1 eV) and to the fully sp^3 C hybridization of saturated organic chains (as compared with the mixed sp^2–sp^3 hybridization of the a-C surface). A wide loss band centered at 20 eV also appears for grazing emission. This set of data indicates that the bulk component (near 28 eV) changes weakly as a function of the emission angle. In contrast, the intensity of the loss component in the range 15–25 eV roughly tracks that of the ester (O–C═O) feature, which is qualitatively consistent with its attribution to surface losses.

For each emission angle, a decomposition of $J(E)$ data (in the range 10–35 eV) has been performed, using the sum of three Gaussians, as illustrated in Fig. 6 ($\alpha = 55^\circ$). The Gaussian line at 28 eV corresponds to the bulk σ + π plasmon, while the Gaussian lines at 19.5 and 13 eV have a different physical origin. The fitting was performed with fixed positions for the bulk plasmon ($\hbar\omega_{BULK} = 28$ eV, fitted FWHM = 16.2 ± 0.6 eV) and for the intermediate Gaussian ($\hbar\omega_{SURF} = 19.5$ eV, fixed FWHM = 9.5 eV). The fitted energy of the third weak component is nearly constant, $\hbar\omega = 13.4 \pm 0.7$ eV.

Using this accurate decomposition, the integrated intensity of the surface loss at 19.5 eV, A_{SP}, has been normalized either to the bulk plasmon loss intensity, A_{BP}, or to the elastic peak intensity, A_{EL}. The inset in Fig. 6 shows a linear variation of both (A_{SP}/A_{BP}) and (A_{SP}/A_{EL}) with $(\cos\alpha)^{-1}$, as verified in previous experiments [72], while the bulk plasmon relative intensity remains unchanged for increasing α values. This decomposition indicates that loss features around 20 eV can be attributed to a surface mechanism; it forms the basis of a more detailed analysis in Section 4.4, in order to separate bulk and surface losses without *a priori* assumptions on the shape of the loss energy distributions.

4.4. Derivation of bulk and surface loss distributions

Fig. 7 reveals a systematic increase in the total loss intensity as a function of increasing emission angle, α, for as-grown and grafted a-C surfaces, with different amplitudes depending on the considered spectral range. The largest difference is observed for the a-C surface covalently grafted with a densely packed molecular layer (surface coverage $\Sigma_{ML} = 3.7 \times 10^{14}\,cm^{-2}$) and it

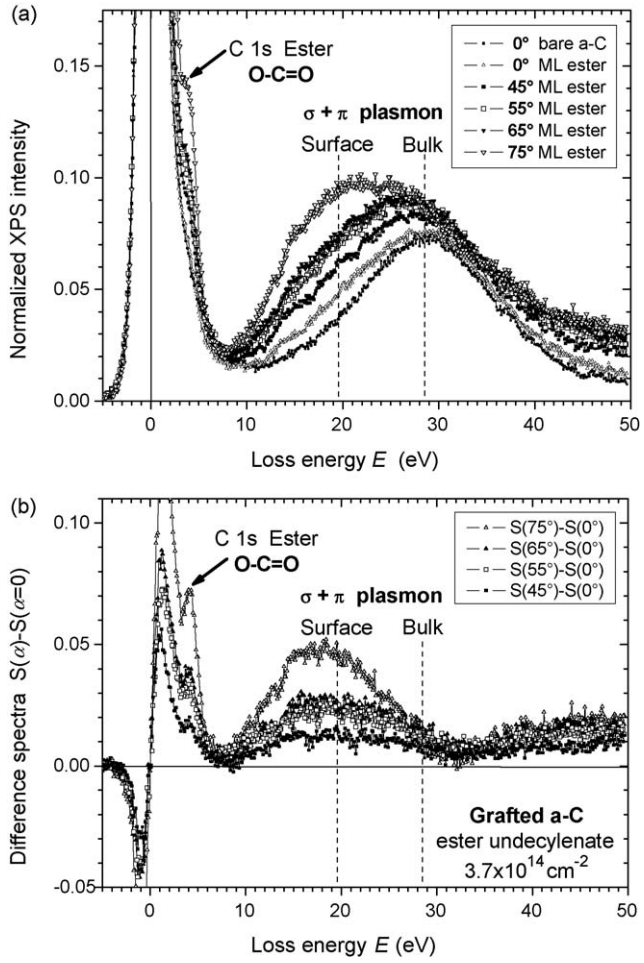

Fig. 5. Angular dependence of the C1s photoelectron loss spectrum for a PLD a-C film grafted with an ester-functionalized molecular layer (surface coverage $\Sigma_{ML} = 3.7 \times 10^{14}\,cm^{-2}$): (a) measurements at $\alpha = 0$, 45, 55, 65, 75°; (b) difference spectra $J(\alpha) - J(\alpha = 0^\circ)$.

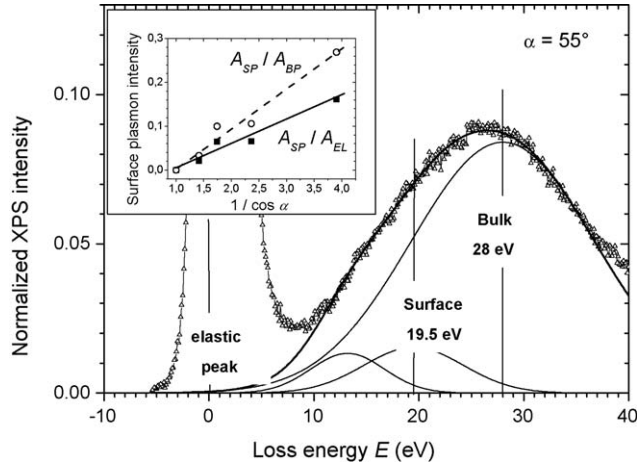

Fig. 6. Decomposition of the C1s photoelectron loss distribution at $\alpha = 55^\circ$ for the ester-functionalized molecular layer (coverage $\Sigma_{ML} = 3.7 \times 10^{14}\,cm^{-2}$) into Gaussian lines corresponding to the bulk σ + π plasmon (28 eV) and to surface components at 19.5 eV and 13 eV. Inset: intensity of the surface plasmon excitation at 19.5 eV normalized to the bulk plasmon (A_{SP}/A_{BP}) and to the elastic peak (A_{SP}/A_{EL}) vs ($1/\cos\alpha$).

is followed by the PFD-grafted surface (surface coverage Σ_{ML} = 2×10^{14} cm^{-2}).

Several factors may affect the magnitude of energy losses, including inaccurate background subtraction, inaccurate position of the zero loss energy, and superposition of multiple losses to single bulk plasmon loss: (i) The difference spectrum equal to zero in annealing experiments (Fig. 3) gives evidence that the background subtraction does not introduce any spurious features in the loss energy range between 10 eV and 50 eV. (ii) Near the zero-loss peak, sharp derivative-like features are highly dependent on the correct alignment of the C1s peak positions; since small shifts may result from changes in the band bending at the a-C film surface, changes in the $sp^3/(sp^2 + sp^3)$ fraction may be difficult to quantify; however this does not affect the plasmon loss analysis. (iii) In the case of multiple volume losses ($n\hbar\omega_P$) the primary electron suffers repeated single processes, spatially separated. Multiple surface losses do not occur since the photoelectrons cross the surface only once. Multiple bulk losses are negligible up to 40 eV.

This angular behaviour being observed on several amorphous carbon films, covalently grafted using either a liquid phase or a gas phase process, we tentatively describe the angular dependence of the lineshape of the normalized loss by:

$$J(E) = B(E) + S(E)(\cos\alpha)^{-1} \tag{4a}$$

We recall that $J(E)$ and $B(E)$ both include the elastic peak distribution $Z(E)$. Hence, using the losses at two angles, α_1 and α_2, the extraction of $B(E)$ and $S(E)$ can be obtained through:

$$B(E) = \frac{\cos(\alpha_1)J(E,\alpha_1) - \cos(\alpha_2)J(E,\alpha_2)}{\cos(\alpha_1) - \cos(\alpha_2)} \tag{4b}$$

$$S(E) = \frac{J(E,\alpha_1) - J(E,\alpha_2)}{\cos(\alpha_1)^{-1} - \cos(\alpha_2)^{-1}} \tag{4c}$$

The robustness of the method has been checked for a number of bare and grafted amorphous surfaces. For a given surface, several pairs of angles were used, showing a good reproducibility, within ±0.003 in $B(E)$ and $S(E)$, but the accuracy is better using normal emission and a large exit angle. A large count rate is required in order to keep a reasonable signal-to-noise ratio in both $B(E)$ and $S(E)$.

In the context of increasing losses for XPS glancing emission, our approach differs from the analysis developed in a previous report [68]. In their work, the parametrization of the shape of the universal background function allows to describe accurately the increasing surface loss contribution for metal surfaces, observed at lower kinetic energies and larger emission angles, and to recover a primary spectrum $F(E)$ independent of the exit angle. In contrast our analysis considers a constant shape of the background function, and does not make any hypothesis on the energy distribution of surface losses.

The validity of the parameterization described by Eq. (4a) has been checked using labelling experiments. For grafted a-C surfaces, the signature of the surface labelling functionality (marked with a star in the measured spectra) is completely suppressed in the distribution of bulk losses, $B(E)$, as evidenced by the lowest curves in Fig. 7a and b (also shown in Fig. 8a, linear scale).

In Fig. 8a, the bulk plasmon distributions derived from all three surfaces are very similar, meaning that the thermal grafting processes do not affect the subsurface region of a-C films. The bulk plasmon distribution can be accurately fitted with a Gaussian function (FWHM ≈ 12–14 eV) in order to estimate its integrated intensity, A_{BP}. Note that the apparent width (2.0 eV ≤ FWHM ≤ 2.2 eV) of the elastic peak corresponding to the primary photoelectrons does not affect the very broad bulk plasmon features (FWHM ≈ 12–14 eV). The bulk plasmon energy is slightly

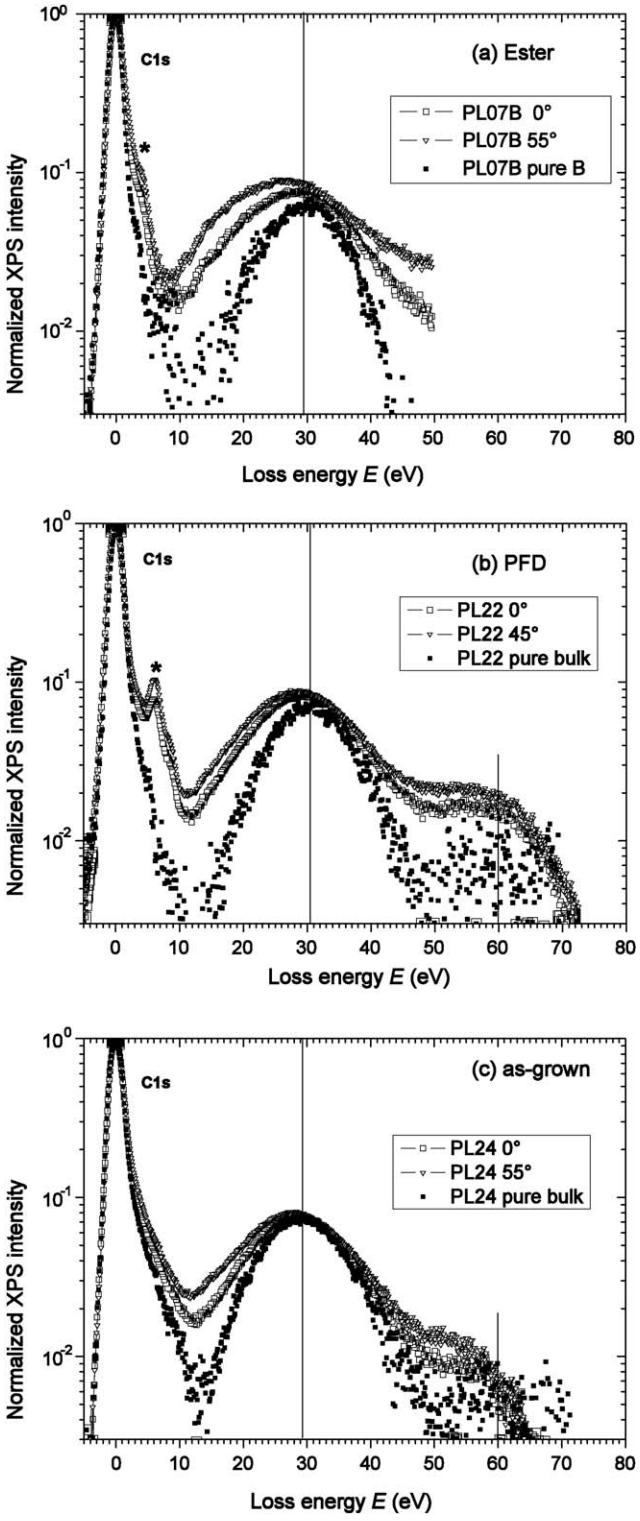

Fig. 7. Dependence of the total plasmon losses of C1s photoelectrons on the emission angle in PLD a-C films: (a) a-C with the ester grafted molecular layer (coverage $\Sigma_{ML} = 3.7 \times 10^{14}$ cm^{-2}); (b) a-C with the PFD immobilized layer (coverage $\Sigma_{ML} = 2.0 \times 10^{14}$ cm^{-2}); (c) as-grown sp^3-rich PLD a-C. The emission angles are given in the respective labels.

larger than the apparent value which can be derived from uncorrected spectra. It is found at $\hbar\omega_{max} = 29.5 \pm 0.2$ eV, for pristine and ester grafted surfaces, while a large value, $\hbar\omega_{max} = 30.5$ eV, is observed for the PFD-grafted a-C surface. A broad second order bulk loss can be detected near 60 eV (Fig. 7b) with a very small probability.

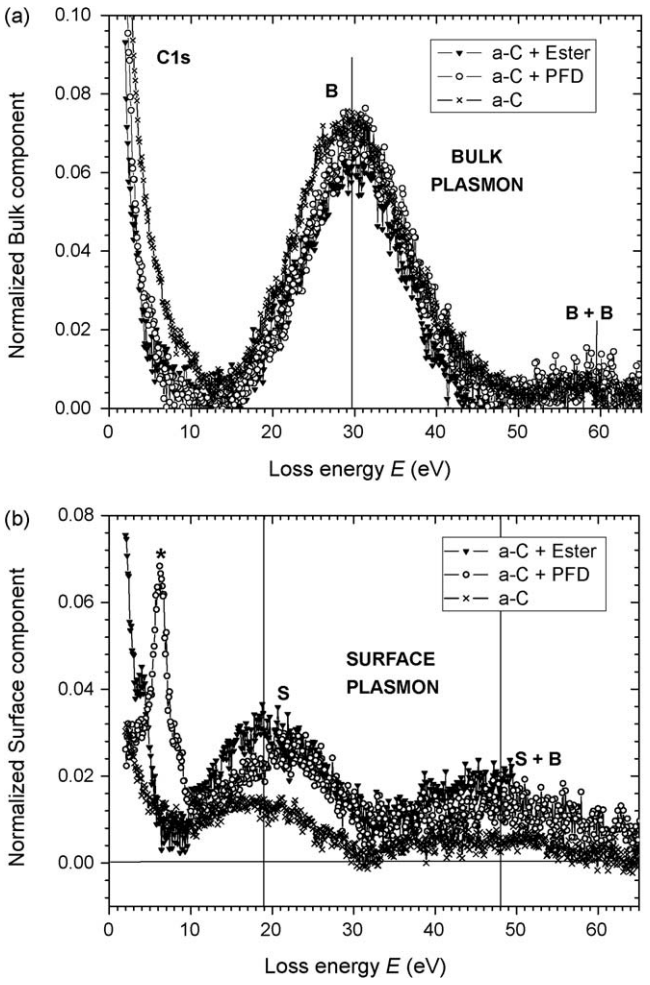

Fig. 8. Pure bulk $B(E)$ (a) and pure surface $S(E)$ (b) loss contributions for the same a-C films as in Fig. 7 (derived from angular C1s losses using Eq. (4a)).

Pure surface components are observed in Fig. 8b, including the labelling functionalities (O=C–O or CF_2), the first-order surface plasmon (S) near 19 eV, and a small second-order surface plasmon (S + B) arising from photoelectrons having previously exchanged a bulk plasmon. The first-order surface plasmon (S) contributes to a significant broadening of the apparent loss towards low energies, as shown in Fig. 7. The surface losses (S + B) have a dominant contribution to the residual loss intensity (≈0.01) observed above 45 eV (Fig. 2).

4.5. Bulk density and plasmon inelastic mean free path

Previous interest in plasmon losses has been focused essentially on the bulk plasmon peak energy to derive the electron density and the atom density of a-C films as a function of the hybridization, $sp^3/(sp^2 + sp^3)$ [15,16,22,23]. In this work, we also address the integrated intensity of the single plasmon loss distribution that is related to the plasmon inelastic mean free path. However, the shape of the loss distribution (related to the dielectric function) remains beyond the scope of this work.

Considering the quasi-free electron model developed for semiconductors [23], the plasmon energy, $E_P = 29.5 \pm 0.2$ eV, is related to an atom density of 1.36×10^{23} at cm^{-3} corresponding to a mass density $\rho_{a\text{-}C}$ (plasmon) = 2.71 g cm^{-3}. As expected, the density derived from the surface sensitive XPS loss technique is slightly smaller than the density obtained from the bulk XRR analysis [49], $\rho_{a\text{-}C}$ (XRR) = 2.93 g cm^{-3}. This is consistent with a larger sp^2 C atom fraction at the extreme surface.

Table 1
Relative intensities, positions and widths of the bulk and surface plasmon losses derived from angular analysis using Eq. (4a) (normalized to the C1s elastic peak) for different PLD a-C films: (a) sp^3-rich PLD a-C, (b) PFD immobilized layer (coverage $\Sigma_{ML} = 2.0 \times 10^{14}$ cm^{-2}), (c) ester grafted molecular layer (coverage $\Sigma_{ML} = 3.7 \times 10^{14}$ cm^{-2}). Parameter a is derived from Eq. (5).

Amorphous carbon	Bulk plasmon			Surface plasmon			
	(A_{BP}/A_{EL})	E_B	W_{BP}	(A_{BP}/A_{EL})	E_{SP}	W_{SP}	(a)
As-deposited a-C (150 mJ)	0.437	29.3	13.5	0.085	17.6	14.6	2.04
PFD grafted a-C (150 mJ)	0.417	30.5	13.0	0.187	21.1	16.1	0.81
Ester grafted a-C (180 mJ)	0.362	29.6	12.2	0.225	19.7	15.4	0.64

The integrated plasmon loss normalized to the elastic peak area provides the ratio $(A_{BP}/A_{EL}) = \lambda/\lambda_P$ (Eq. (3)). For XPS excitation with a Mg Kα ($h\nu = 1253.6$ eV) source, the kinetic energy of C1s photoelectrons ($E_0 \approx 970$ eV) in graphite or amorphous carbon corresponds to a characteristic inelastic mean free path λ = 1.6 nm [73]. From the average ratio $(A_{BP}/A_{EL}) = 0.405$ (Table 1) found in C1s core level spectra, a typical value of $\lambda_P = 4.0 \pm 0.4$ nm is experimentally obtained for the plasmon inelastic mean free path in PLD a-C films. This value of λ_P is an upper limit because the area (A_{EL}) of the elastic peak can be slightly overestimated due to the tail of electron–electron losses observed in the range 0–10 eV (e.g. in Fig. 7c, pure bulk component of the bare a-C surface).

4.6. Surface excitation parameter

The modified Oswald equation [56,57] relates the SEP (surface plasmon loss intensity, A_{SP}, divided by the elastic peak intensity, A_{EL}) to the emission angle through the photoelectron energy E_0 and a material-dependent constant a:

$$\frac{A_{SP}}{A_{EL}} = (1 + 0.173a(E_0)^{1/2}\cos\alpha)^{-1} \quad (5)$$

The effect of the factor (cos α) is due to the strong interaction of the electrons hitting the surface at grazing incidence compared with that of an electron at normal incidence [35]. Different expressions were also proposed for estimation of the SEP [65–67].

Using the experimental values of (A_{SP}/A_{EL}) reported in Table 1 and $E_0 \approx 970$ eV, the characteristic parameter for the pristine a-C surface is $a = 2.0 \pm 0.5$. This large value of parameter a explains why surface plasmon losses in amorphous semiconductors are seldomly observed. In contrast, small SEP values are obtained for the PFD-grafted ($a = 0.81 \pm 0.2$) and ester grafted ($a = 0.64 \pm 0.1$) a-C surfaces, being closer to usual values found for nearly free-electron materials, for which the Oswald derivation is given, such as Al ($a = 0.7$), Ge ($a = 0.9$) and Si ($a = 1.0$) [56,57,66,67].

4.7. Discussion

Another plausible explanation for the increase of losses at about 20 eV for grated a-C surfaces is the fact that these "polymeric-like" surfaces display bulk plasmon features at these energies that are enhanced in the measured spectra because of their location at the top-most surface layer. Two independent experiments have been performed to check this possibility.

The expected bulk plasmon loss energy for the ester molecular monolayer, immobilized on the amorphous carbon surface, can be derived from grazing angle X-ray reflectometry measurements. A 35 nm-thick a-C film grown in identical conditions was grafted with a coverage of $\Sigma_{ML} = 3.5 \pm 0.4 \times 10^{14}$ cm^{-2}; the densities of the

a-C film, $\rho_{OML} = 2.86 \pm 0.05$ g cm^{-3} and the molecular layer, $\rho_{OML} = 1.08 \pm 0.05$ g cm^{-3}, were fitted with a multilayer model, including interface roughness [49]. Hence a ratio of 1.63 is expected between their respective bulk plasmon energies; using $E_P = 29.5$ eV for a-C, the bulk component of the molecular layer should be close to $E_P = 18 \pm 1$ eV. The experimental values reported in Table 1, corresponding to Fig. 8b, are found at 19.7 and 21.1 eV, i.e. above the expected range.

A complementary experiment has been performed by grafting a perfluorodecene monolayer on a smooth amorphous silicon film (coverage $\Sigma_{ML} = 2.6 \times 10^{14}$ cm^{-2}) [74]. In this case, for Si 2p photoelectrons, the pure bulk loss of amorphous silicon is located at 17 eV, as expected; a very small surface component is located near 12 eV. Difference spectra S(a-Si:H + PFD) − S(a-Si:H) show a small signal near 19 eV which contribution to the (A_{SP}/A_{EL}) ratio is smaller than 0.05. The latter signal (at energies larger than the bulk a-Si plasmon) may be the signature of the PFD monolayer; its intensity is five times less than the (A_{SP}/A_{EL}) value observed for a-C surfaces with immobilized molecular monolayers. This result indicates that bulk losses in ultra thin films (such as molecular monolayers) are not very efficient. In conclusion, the increasing loss observed for glancing photoelectron emission is attributed to the a-C surface plasmon loss rather than to the molecular monolayer bulk loss.

Finally, it is important to mention that bulk and surface losses are considered disregarding their origin (intrinsic, extrinsic). Previous calculations based on the dielectric model for photoelectron spectroscopy [60] have shown that the angular dependence of these intrinsic and extrinsic losses might not be identical. These calculations for Al provide a very asymmetric bulk plasmon loss at normal emission, arising from a very strong intrinsic loss. In contrast, our results obtained with a-C at normal emission give evidence of a rather symmetrical loss, either in raw measurements or after elimination of the surface contribution derived from our parametrization. Hence, for some unknown reason, the relative contribution of intrinsic losses may be much smaller in our experiments. As far as surface losses are concerned, the calculated relative contribution of the intrinsic component is negligible [60].

5. Conclusion

Bulk and surface $\sigma + \pi$ plasmon excitations have been derived from core level loss spectra obtained as a function of the photoelectron emission angle, using a conventional XPS instrument. In this work, sp^3-rich and atomically smooth PLD a-C surfaces were used in their as-grown state, after UHV annealing and after covalent immobilization of a molecular monolayer, either perfluorinated or labelled with an ester functionality.

As compared with the pristine a-C surface, C1s spectra of the grafted surfaces display a much larger loss for a broad range of loss energies (15–25 eV) located at lower values than the bulk $\sigma + \pi$ plasmon loss centered at 29.5 eV. This larger loss intensity is not observed after UHV annealing of a-C; hence it cannot be attributed to the thermal treatment itself. In addition, grafted surfaces show a strong enhancement of the total loss probability as the photoelectron emission approaches grazing incidence, which indicates that surface plasmon losses become dominant.

The determination of the bulk plasmon energy from XPS spectra is useful to characterize the near-surface electron density. We have shown that all core level loss spectra contain a significant surface plasmon contribution that needs to be removed for an accurate estimation of the electron density.

A simple parameterization has been proposed to separate bulk and surface excitations using variable emission angle XPS measurements, without *a priori* assumptions on the shape of the loss energy distributions. The validity of Eq. (4a), which assumes that the angular dependence of the surface loss contribution increases as $(\cos\alpha)^{-1}$, has been checked using the labelling functionalities immobilized on the a-C surface. Note that high electron density materials (including PLD a-C) are well suited for such analysis because the overlap between the core level peak and the surface loss distribution is small.

It is well known that the properties of surface plasmons are sensitive to modifications of the surface, such as coating of the boundary with a thin film of another dielectric function, or a change of the geometry of the boundary (roughness, grating structure) [35,63,75]. However for high quality surfaces, other parameters may affect the plasmon loss probability. It should be noted that the orientation of the dipole moments of the molecules relative to the electric field of the surface plasmon affects the interaction probability [76]; hence one can expect a variation of the surface plasmon loss with orientation (ordering) of the molecular layer.

Interestingly, in this study we observe that the relative intensity of the surface plasmon loss (SEP) increases with the molecular coverage of the amorphous carbon surface, without a significant change in the bulk loss probability; it is close to the values usually found for clean semiconductor or metal surfaces. In our grafting studies with amorphous carbon surfaces, the molecular ordering cannot arise from the substrate order but should rather be attributed to van der Waals interactions between molecules. More work is required to compare the surface plasmon signature with other techniques sensitive to molecular ordering.

Acknowledgments

The authors acknowledge several colleagues at University of Rennes 1: Bruno Fabre (MaCSE) for liquid phase grafting experiments, Sophie Ollivier (LCSIM) for AFM characterizations, Joseph Le Lannic (CMEBA) for SEM measurements, Stéphanie Députier (LCSIM) for PLD deposition, André Perrin and Maryline Guilloux-Viry (LCSIM) for useful discussions. One of us (D.D.) is grateful to University of Rennes 1 for a grant as an invited professor.

References

[1] J. Robertson, Mater. Sci. Eng. R 271 (2002) 1–153.
[2] S. Muhl, J.M. Mendez, Diamond Relat. Mater. 8 (10) (1999) 1809.
[3] N. Hellgren, M.P. Johansson, E. Broitman, L. Hultman, J.-E. Sundgren, Phys. Rev. B: Condens. Matter 59 (1999) 5162.
[4] T.A. Friedmann, J.P. Sullivan, J.A. Knapp, D.R. Tallant, D.M. Follstaedt, D.L. Medlin, P.B. Mirkarimi, Appl. Phys. Lett. 71 (1997) 3820.
[5] R. Hauert, Diamond Relat. Mater. 12 (2003) 583–589.
[6] S.E. Rodil, R. Olivares, H. Arzate, S. Muhl, Diamond Relat. Mater. 12 (3–7) (2003) 931..
[7] H. Cachet, C. Deslouis, M. Chouiki, B. Saidani, N.M.J. Conway, C. Godet, J. Electrochem. Soc. 149 (2002) E233.
[8] K. Lmimouni, C. Legrand, C. Dufour, A. Chapoton, C. Belouet, Appl. Phys. Lett. 78 (2001) 2437.
[9] B. Sun, P.E. Colavita, H. Kim, M. Lockett, M.S. Marcus, L.M. Smith, R.J. Hamers, Langmuir 22 (2006) 9598.
[10] S. Ababou-Girard, H. Sabbah, B. Fabre, K. Zellama, F. Solal, C. Godet, J. Phys. Chem. C 111 (2007) 3099.
[11] J. Robertson, Diamond Relat. Mater. 14 (2005) 942;
J. Robertson, Diamond Relat. Mater. 2 (1993) 984.
[12] S. Uhlmann, T. Frauenheim, Y. Lifshitz, Phys. Rev. Lett. 81 (1998) 641.
[13] J. Fink, Th. Müller-Heinzerling, J. Pflüger, B. Scheerer, B. Dischler, P. Koidl, A. Bubenzer, R.E. Sah, Phys. Rev. B 30 (1984) 4713.
[14] D.R. McKenzie, D. Muller, B.A. Pailthorpe, Phys. Rev. Lett. 67 (1991) 773.
[15] P.J. Fallon, V.S. Veerasamy, C.A. Davis, J. Robertson, G.A.J. Amaratunga, W.I. Milne, J. Koskinen, Phys. Rev. B 48 (1993) 4777.
[16] J. Kulik, Y. Lifshitz, G.D. Lempert, J.W. Rabalais, D. Marton, J. Appl. Phys. 76 (1994) 5063.
[17] J. Kulik, G.D. Lempert, E. Grossman, D. Marton, J.W. Rabalais, Y. Lifshitz, Phys. Rev. B 52 (1995) 15812.
[18] S.T. Jackson, R.G. Nuzzo, Appl. Surf. Sci. 90 (1995) 195.

[19] P. Reinke, M.G. Garnier, P. Oelhafen, J. Electr. Spectrosc. Relat. Phenom. 136 (2004) 239.
[20] L. Calliari, M. Filippi, N. Laidani, M. Anderle, J. Electr. Spectrosc. Relat. Phenom. 150 (2006) 40.
[21] V.J. Rico, F. Yubero, J.P. Espinos, J. Cotrino, A.R. Gonzalez-Elipe, D. Garg, S. Henry, Diamond Relat. Mater. 16 (2007) 107.
[22] A. LiBassi, A.C. Ferrari, V. Stolojan, B.K. Tanner, J. Robertson, L.M. Brown, Diamond Relat. Mater. 9 (2000) 771.
[23] A.C. Ferrari, A. Libassi, B.K. Tanner, V. Stolojan, J. Yuan, L.M. Brown, S.E. Rodil, B. Kleinsorge, J. Robertson, Phys. Rev. B 62 (2000) 11089.
[24] T.J. Bernatowicz, P.C. Gibbons, R.S. Lewis, Astrophys. J. 359 (1990) 246.
[25] P. Reinke, J.E. Klemberg-Sapieha, L. Martinu, J. Appl. Phys. 76 (1994) 5754.
[26] G. Francz, P. Reinke, P. Oelhafen, W. Hänni, Thin Solid Films 270 (1995) 200.
[27] M. Zarrabian, N. Fourches-Coulon, G. Turban, M. Lancin, C. Marhic, Diamond Relat. Mater. 9 (2000) 722.
[28] S.R.P. Silva, V. Stolojan, Thin Solid Films 488 (2005) 283.
[29] J. Daniels, C.v. Festenberg, H. Raether, K. Zeppenfeld, Springer Tracts in Modern Physics, vol. 54, Springer-Verlag, Berlin, 1970, p. 77.
[30] J. Neufeld, R.H. Ritchie, Phys. Rev. 98 (1955) 1632.
[31] R.H. Ritchie, Phys. Rev. 106 (1957) 874.
[32] H. Raether, Solid State Excitations by Electrons, Springer Tracts in Modern Physics, vol. 38, Springer-Verlag, Berlin, 1965, p. 84.
[33] D.R. Penn, Phys. Rev. Lett. 38 (1977) 1429.
[34] P. Steiner, H. Höchst, S. Hüfner, Z. Phys. B 30 (1978) 129.
[35] R.F. Egerton, Electron Energy Loss Spectroscopy in the Electron Microscope, Plenum Press, 1996.
[36] H. Raether, Excitation of Plasmons and Interband Transitions by Electrons, Springer Tracts in Modern Physics, vol. 88, Springer-Verlag, Berlin, 1997.
[37] V. Stolojan, Amorphous Carbon and its properties, in: S.R.P. Silva (Ed.), EMIS Datareviews Series, 29, INSPEC, 2002, p. 83.
[38] S. Waidmann, M. Knupfer, J. Fink, B. Kleinsorge, J. Robertson, Diamond Relat. Mater. 9 (2000) 722.
[39] Y. Ohno, Phys. Rev. 39 (1989) 8209.
[40] P. Kovarik, E.B.D. Bourdon, R.H. Prince, Phys. Rev. B 48 (1993) 12123.
[41] F. Barreca, A.M. Mezzasalma, G. Mondio, F. Neri, S. Trusso, Thin Solid Films 398–399 (2001) 228.
[42] F. Barreca, A.M. Mezzasalma, G. Mondio, F. Neri, S. Trusso, C. Vasi, Thin Solid Films 377–378 (2000) 631.
[43] C.A. Davis, G.A.J. Amaratunga, K.M. Knowles, Phys. Rev. Lett. 80 (1998) 3280.
[44] J.C. Lascovitch, S. Scaglione, Appl. Surf. Sci. 78 (1994) 17.
[45] J. Schäfer, J. Ristein, R. Graupner, L. Ley, U. Stephan, T. Frauenheim, V.S. Veerasamy, G.A.J. Amaratunga, M. Weiler, H. Ehrardt, Phys. Rev. B 53 (1996) 7762.
[46] A. Zebda, H. Sabbah, S. Ababou-Girard, F. Solal, C. Godet, Appl. Surf. Sci. 254 (2008) 4980–4991.
[47] M.M. Guraya, H. Ascolani, G. Zampieri, J.I. Cisneros, J.H. Dias da Silva, M.P. Cantao, Phys. Rev. B 42 (1990) 5677–5684.
[48] K.J. Gruntz, L. Ley, R.L. Johnson, Phys. Rev. B 24 (1981) 2069–2081.
[49] H. Sabbah, S. Ababou-Girard, B. Fabre, F. Solal, C. Godet, Diamond Relat. Mater., in press.
[50] D.A. Shirley, Phys. Rev. B 5 (1972) 4709.
[51] S. Tougaard, Surf. Interface Anal. 11 (1988) 453.
[52] S. Tougaard, Surf. Interface Anal. 25 (1997) 137.
[53] M.P. Seah, Surf. Sci. 420 (1999) 285.
[54] M.P. Seah, Surf. Sci. 471 (2001) 185.
[55] D.P. Woodruff, T.A. Delchar, Modern Techniques of Surface Science, second ed., Cambridge University Press, 1994.
[56] N. Pauly, S. Tougaard, F. Yubero, Surf. Interface Anal. 37 (2005) 1151.
[57] N. Pauly, S. Tougaard, F. Yubero, Surf. Interface Anal. 38 (2006) 672.
[58] F. Yubero, S. Tougaard, Phys. Rev. B 46 (1992) 2486.
[59] A.C. Simonsen, F. Yubero, S. Tougaard, Phys. Rev. B 56 (1997) 1612.
[60] F. Yubero, S. Tougaard, Phys. Rev. B 71 (2005) 045414.
[61] G. Mondio, F. Neri, S. Patane, A. Arena, G. Marletta, F. Iacona, Thin Solid Films 207 (1992) 313.
[62] Z.L. Wang, Micron 27 (1996) 265.
[63] C. Denton, J.L. Gervasoni, R.O. Barrachina, N.R. Arista, Phys. Rev. B 57 (1998) 4498.
[64] F. Paumier, et al. Mater. Sci. Eng. A 422 (2006) 29.
[65] Y.F. Chen, Surf. Sci. 380 (1997) 199.
[66] W.S.M. Werner, W. Smekal, C. Tomastik, H. Stori, Surf. Sci. 486 (2001) L461–466.
[67] W.S.M. Werner, Surf. Interface Anal. 31 (2001) 141.
[68] A.C. Simonsen, F. Yubero, S. Tougaard, Surf. Sci. 436 (1999) 149.
[69] H. Sabbah, S. Ababou-Girard, C. Godet, F. Solal, unpublished.
[70] T. Katsuno, C. Godet, J.C. Orlianges, A.S. Loir, F. Garrelie, A. Catherinot, Appl. Phys. A 81 (2005) 471–476.
[71] J.L. Figueiredo, M.F.R. Pereira, M.M.A. Freitas, J.J.M. Orfao, Carbon 37 (1999) 1379.
[72] C.J. Powell, Phys. Rev. 175 (1968) 511.
[73] C.J. Powell, A. Jablonski, NIST Electron Inelastic-Mean-Free-Path, Database version 1.1, 2000.
[74] H. Sabbah, J.P. Conde, V. Chu, A. Zebda, S. Ababou-Girard, F. Solal, C. Godet, J. Appl. Phys., in press.
[75] T. Nagatomi, R. Shimizu, R.H. Ritchie, J. Appl. Phys. 85 (1999) 4231.
[76] J. Dintinger, S. Klein, T.W. Ebbesen, Adv. Mater. 18 (2006) 1267–1270.